Journal of Aerosol Science 114 (2017) 263–275

Contents lists available at ScienceDirect

Journal of Aerosol Science

journal homepage: www.elsevier.com/locate/jaerosci

Numerical investigation on non-steady-state filtration of elliptical fibers for submicron particles in the "Greenfield gap" range

Haokai Huang, Chaohe Zheng, Haibo Zhao*

State Key Laboratory of Coal Combustion, School of Energy and Power Engineering, Huazhong University of Science and Technology, Wuhan 430074, China

ARTICLE INFO

Keywords:
Lattice Boltzmann method
Elliptical fiber
Particle loading
Three-dimensional simulation
High-efficiency filtration

ABSTRACT

While noncircular fibers (especially elliptical fibers) have demonstrated significant advantage of high collection efficiency for fine particles, only a few investigations have yet been conducted to study the non-steady-state filtration performance of noncircular fibers during the particle deposition process. In this work, we utilize a lattice Boltzmann-cellular automata (LB-CA) probabilistic model to investigate the growing process of particle dendrites on elliptical fibers. The transient pressure drop and collection efficiency are analyzed. For the deposition of sub-micron particles (0.3–0.5 μm in the "Greenfield gap" range) which are dominated by the diffusion and interception mechanism, the captured particles distribute relatively uniformly around elliptical fibers (the equivalent diameter d_f of 22.8 μm and the packing density of 5% in this work) at the initial stage of loading process. The deposited particle leads to the formation of complicated dendrites, expanding the filtration area and thereby altering the flow field. Then particles will mostly deposit on the windward of the elliptical fibers (especially on the both ends of the elliptical long axis) at the complete dendrites capture stage. Various operation conditions (inlet flow velocity of 0.1–0.3 m/s, particle diameter of 0.3–0.5 μm, aspect ratio of elliptical fibers of 2–4, orientation angle of 30°~60°) are simulated. It is found that the pressure drop of dust loaded elliptical fibers normalized by the corresponding pressure drop of clean elliptical fibers increases almost exponentially with the mass of captured particles; and the normalized collection efficiency of elliptical fibers is approximately a linear function of the deposit mass when the increase rate of the normalized efficiency is stabilized.

1. Introduction

Fine particles suspended in the air cause adverse impact on the environment, climate and human health, which is one of the largest environmental problems. Fibrous filters are widely used in coal-fired power plants, chemical engineering processes, heating and semiconductor industries because of the advantages of low price, high collection efficiency of fine particles and simple construction for filter regeneration. The filtration process of fibrous filters contains complicated flow-particle-fiber interactions. Brownian diffusion, interception and inertial impaction are three basic mechanisms that lead to an aerosol particle deposits on a neutral fiber (Ramarao, Tien, & Mohan, 1994). In the present work, the deposition process of sub-micron particles (diameter of 0.3–0.5 μm in the "Greenfield gap" range (Greenfield, 1957)) is considered, and the effect of inertial impaction can be neglected while diffusion and interception are the dominant filtration mechanisms.

Classical fibrous filtration theories, which were based on a numerical or an exact solution of the velocity distribution of the flow

* Corresponding author.
E-mail address: hzhao@mail.hust.edu.cn (H. Zhao).

http://dx.doi.org/10.1016/j.jaerosci.2017.09.018
Received 2 May 2017; Received in revised form 9 August 2017; Accepted 14 September 2017
Available online 29 September 2017

around a circular fiber in a two-dimensional configuration, were originally developed for clean media. Based on these theories, a number of expressions for calculating the pressure drop and collection efficiency of fibrous filters have been proposed (Brown, 1993). However, the clean condition only exists in the initial stage of the filtration process for a short time, which can be regarded as the steady-state filtration. As for the real fibrous filtration process, when particles move to the surface of fibers, they may deposit on the fiber, increasing the collection area and thereby altering the flow field. The formation of particle dendrites will exert significant effects on the capture efficiency and pressure drop.

It has been identified in previous studies that the formation of dendrites follow three stages of dendrite formation—initial fiber collection, interim fiber-dendrite collection, and complete dendrite collection (Li & Marshall, 2007). However, simulation of this dynamic process is still difficult for several reasons: particle dendrites growth on dust loaded fibers is complicated and does not follow simple geometrical patterns; the shape of particle dendrites changes depending strongly upon the dominant capture mechanism; the growth of particle dendrites will change the boundary conditions for flow field and the flow field around the fiber needs to be recalculated after particle deposition.

Billings (1996) was probably the first to perform a systematic investigation of particle accumulation on individual fiber. He calculated the single fiber efficiency from SEM micrographs taken at regular time intervals. Payatakes and Tien (1976) studied the formation of dendrites on fibers uniformly placed within a Kuwabara cell in the interception regime. Payatakes and Gradoń (1980) expanded this model to simulate the filtration process of fibers in the diffusion and inertial impaction regimes. Kanaoka, Emi, and Myojo (1980) studied the growing process of particle dendrites on a fiber and the time dependency of single fiber collection efficiency utilizing Monte Carlo simulation technique. They found that the ratio of collection efficiency under dust loading (η) to that of the clean fiber (η_0) is approximately linear with the mass of deposited particles (m): $\eta/\eta_0 = 1 + \lambda m$, where λ is the increase rate of the normalized collection efficiency. Then, Myojo, Kanaoka, and Emi (1984) experimentally confirmed the theoretical investigations of Kanaoka et al. (1980) in the region of inertial and interception mechanisms, and found that the collection efficiency is more sensitive to Stokes number than interception parameter. In addition, Kanaoka and Hiragi (1990) proposed a model to predict the pressure drop of dust loaded filter based on the direct microscopic observation of particle attachment processes. Zhao, Tardos, and Pfeffer (1991) experimentally studied both the pressure drop and collection efficiency in dust loaded electrostatically filters by replacing the fiber diameter and packing density with the equivalent values. Thomas et al. (1999), Thomas, Penicot, Contal, Leclerc, and Vendel (2001) proposed a new model to give a quantitative prediction of pressure drop increase during filter clogging through dividing the filter into various slices in which two kinds of particle collectors coexist. Based on these researches, many numerical simulations (Przekop & Gradoń, 2008; Przekop, Moskal, & Gradoń, 2003) and experimental measurements (Kasper, Schollmeier, Meyer, & Hoferer, 2009; Kasper, Schollmeier, & Meyer, 2010) were conducted to investigate the dust loading problems.

With the fast development of manufacturing technology and materials science, fibrous filters composed of noncircular fibers have been used in practical applications to meet different requirements. A series of noncircular fibers have been commercially produced for high performance specialty nonwoven fabrics (*e.g.*, spun-bonded trilobal fibers with the brand name REEMAY registered by BBA Fiberweb). Having the advantage of larger specific surface area than traditional circular ones, the noncircular fibers demonstrate great potential to make fibrous filters at advantages of collection efficiency, particle loading capacity, manufacturing flexibility and mechanical strength. Many researchers have investigated the filtration performance of elliptical fibers (Raynor, 2002; Wang, Zhao, & Wang, 2014) and of rectangular fibers (Adamiak, 1999; Fardi & Liu, 1992; Ouyang & Liu, 1998; Zhu, Lin, & Cheung, 2000). The other kinds of noncircular fibers with triangle and trilobal cross-sections have also been studied (Fotovati, Tafreshi, & Pourdeyhimi, 2011; Inagaki, Sakai, & Namiki, 2001; Lamb & Costanza, 1980; Sanchez, Rodriguez, & Alvaro, 2007). There are some articles focusing on comparing the filtration performance of fibers with different cross-sections (Hosseini & Tafreshi, 2011; Huang, Wang, & Zhao, 2016; Wang & Zhao, 2015). In our recent work (Huang et al., 2016), diffusional capture efficiency of four kinds of noncircular clean fibers in filtration was quantitatively investigated. It turns out that elliptical fibers demonstrate higher diffusional collection efficiency than the other kinds of noncircular fibers with the same specific surface area. Nevertheless, neither of the above works investigated the non-steady-state filtration processes of noncircular fibers. Our extensive literature search resulted only a few articles (Cheung, Cao, & Yan, 2005; Sanchez et al., 2007) studying the particle loading process of noncircular fibers. The non-steady-state deposition of particles on noncircular fibers is not well understood.

Among different numerical simulation method, lattice Boltzmann method (LBM), which is used to simulate the flow fields, is considered as a very promising approach to treat irregular and dynamic geometrical boundaries like the captured particles forming dendrites here. Filippova and Hänel (1997) used the lattice Boltzmann method to simulate the gas-particle flow and growth of particle dendrites. Their work has taken a significant step towards simulating this complex process. Lantermann and Hänel (2007) used the lattice Boltzmann method to calculate the flow field and electrical potential field and particle Monte Carlo method to study the morphology of deposited particles.

As well-known, very fine particles (< 0.1 μm) and very coarse particles (> 5 μm) can be collected by fibers very efficiently, mainly due to Brownian diffusion and inertial impaction respectively; however, intermediate particles (*e.g.*, 0.3–0.5 μm in diameter) are hardly removed by fibers because the two important filtration mechanisms, Brownian diffusion and inertial impaction, have the minimum effect on these particles and the contribution of interception mechanism on capture efficiency is generally weak. Considering the outstanding performance of elliptical fibers on the effective removal of fine and intermediate particles, our idea is to utilize the elliptical fibers to improve the filtration efficiency of sub-micron particles (0.3, 0.4, and 0.5 μm as representative). In order to attain optimal filtration performance of elliptical fibers with respect to sub-micron particles in the “Greenfield gap” range, it is essential to deeply investigate the loading behavior of elliptical fibers. In the present study, the growing process of particle dendrites on a dust loaded elliptical fiber and the dynamic evolution of both pressure drop and collection efficiency are investigated using a lattice Boltzmann-cellular automata (LB-CA) probabilistic model, which has been already successfully applied by our group (Wang,

Zhao, Guo, & Zheng, 2012; Wang, Zhao, Wang, He, & Zheng, 2013) to simulate particle loading processes of circular fibers. The LB-CA model is good at considering the effect of Brownian diffusion due to its stochastic nature in treating particle motion. By calculating the probability of the movement of solid particles on the same regular lattices as fictitious fluid particles, we can quantitatively describe the detailed motion of particles under the combined effects of drag force and Brownian diffusion. This paper aims at giving a better understanding of the growth of particle dendrites on elliptical fibers and of the dynamic evolution of both pressure drop and collection efficiency. These results are useful for design and optimization of fibrous filter structure. The paper is organized as follows. The simulation method is first described in Section 2. In Section 3.1, boundary condition and simulation details are presented. The formation process of particle dendrites is studied in Section 3.2. The dynamic evolution of both pressure drop and collection efficiency of elliptical fibers during loading is given in Section 3.3. Finally, Section 4 summarizes the findings from this work.

2. The three-dimensional LB-CA simulation for gas-solid two-phase flows

2.1. The standard Lattice Boltzmann model for gas flows

The Lattice Boltzmann method is a very promising method for complex flow simulations. The lattice BGK propagation scheme is derived from the classic Boltzmann equation with the Bhatnagar-Gross-Krook (BGK single-relaxation) collision operator and the evolution equation can be expressed as follows (Qian, D'Humieres, & Lallemand, 1992):

$$f_i(x + \mathbf{c}_i\Delta t,\ t + \Delta t) - f_i(x,\ t) = -\frac{1}{\tau}[f_i(x,\ t) - f_i^{\mathrm{eq}}(x,\ t)], \tag{1}$$

where Δt is the time step, τ is the dimensionless relaxation time, f_i^{eq} is the equilibrium distribution function, the lattice velocities $\mathbf{c}_i$ can be calculated in the *D3Q15* lattice model as:

$$\mathbf{c}_i = \begin{pmatrix} 0 & 1 & -1 & 0 & 0 & 0 & 0 & 1 & -1 & 1 & -1 & 1 & -1 & 1 & -1 \\ 0 & 0 & 0 & 1 & -1 & 0 & 0 & 1 & -1 & 1 & -1 & -1 & 1 & -1 & 1 \\ 0 & 0 & 0 & 0 & 0 & 1 & -1 & 1 & -1 & -1 & 1 & 1 & -1 & -1 & 1 \end{pmatrix} \tag{2}$$

The directions of lattice velocities are shown in Fig. 1, *i.e.*, face-centered directions for $i=1$–6, diagonal directions for $i=7$–14 and zero velocity for $i=0$. The equilibrium distribution function can be expressed as following:

$$f_i^{\mathrm{eq}} = \rho\omega_i\left(1 + \frac{\boldsymbol{c}_i\cdot\boldsymbol{u}}{c_s^2} + \frac{(\boldsymbol{c}_i\cdot\boldsymbol{u})^2}{2c_s^4} - \frac{\boldsymbol{u}^2}{2c_s^2}\right), \tag{3}$$

where $\boldsymbol{u}$ is the macroscopic velocity of local fluid, ρ is the fluid density, ω_i is the weight coefficient related to the lattice model with $\omega_0=2/9$, $\omega_i=1/9$ ($i=1$–6), $\omega_i=1/72$ ($i=7$–14) in the *D3Q15* model, $\boldsymbol{c}_s$ means the local sound speed, $c_s=\sqrt{3}c/3$, and $c=\Delta x/\Delta t$, Δx is the lattice step length.

The kinematic viscosity and fluid pressure are calculated as:

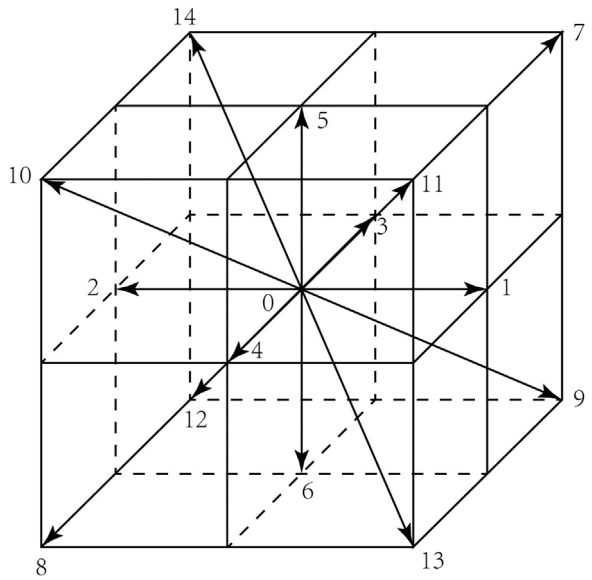

Fig. 1. *D3Q15* model.

$$\begin{cases} \nu = \frac{c_s^2}{2}(2\tau - 1)\Delta t \\ P = \rho c_s^2 \end{cases}. \tag{4}$$

The macroscopic quantities of flow fields can be derived from statistics of distribution function. With the discretized velocity space, the macroscopic density ρ and momentum fluxes ρ**u** can be evaluated as:

$$\rho = \sum_{i=0}^{Q-1} f_i, \quad \rho\mathbf{u} = \sum_{i=0}^{Q-1} f_i \mathbf{c}_i. \tag{5}$$

2.2. CA model for particle motion

The particles motion is described by the Cellular Automata probabilistic model, which was first proposed by Masselot and Chopard (1998). Our group has extended the original model to quantitatively deal with the exact drag force and other external forces acting on the particles (Wang et al., 2012). In this study, the transport of particles is dependent of the combined effect of drag force and Brownian force (Maze, Vahedi Tafreshi, Wang, & Pourdeyhimi, 2007), and the particle motion is governed by the following equation:

$$\frac{\mathrm{d}\boldsymbol{u}_\mathrm{p}}{\mathrm{d}t} = \boldsymbol{F}_\mathrm{D} + \boldsymbol{F}_\mathrm{B} = \frac{\boldsymbol{u} - \boldsymbol{u}_\mathrm{p}}{\tau_\mathrm{p}} + \varsigma\sqrt{\frac{216\mu k_\mathrm{B} T}{\pi\rho_\mathrm{p}^2 d_\mathrm{p}^5 \Delta t}}, \tag{6}$$

where $\boldsymbol{u}_\mathrm{p}$ is the particle velocity, τ_p is the relaxation time of particle, $\tau_\mathrm{p} = C_\mathrm{c}\rho_\mathrm{p} {d_\mathrm{p}}^2/(18\mu)$, μ is the dynamic viscosity of fluid, C_c is the Cunningham slip correction factor, $C_\mathrm{c} = 1 + 2.514\lambda/d_\mathrm{p} + 0.8\lambda/d_\mathrm{p}\cdot\exp(-0.55 d_\mathrm{p}/\lambda)$, λ is the mean free path length of air molecules, $\boldsymbol{F}_\mathrm{D}$ is the drag force, $\boldsymbol{F}_\mathrm{B}$ is the Brownian force, ς is a Gaussian random number with zero mean and a standard deviation of one, d_p is the particle diameter, k_B is the Boltzmann constant and T is the temperature of fluid. It is worth noting that the simulation is able to consider interception naturally, that is, particles are collected when they come within ½ of a particle diameter from a fiber or previously collected particles.

The particle velocity and displacement within one time step can be explicitly calculated through twice integration of Eq. (6):

$$\boldsymbol{u}_\mathrm{p}^{n+1} = \boldsymbol{u}_\mathrm{p}^{n}\exp\left(-\frac{\Delta t}{\tau_\mathrm{p}}\right) + (\boldsymbol{u} + \boldsymbol{F}_\mathrm{B}\tau_\mathrm{p})\left(1 - \exp\left(-\frac{\Delta t}{\tau_\mathrm{p}}\right)\right), \tag{7}$$

$$\boldsymbol{x}_\mathrm{p}^{n+1} = \boldsymbol{x}_\mathrm{p}^{n} + (\boldsymbol{u}_\mathrm{p}^{n} - \boldsymbol{u})\left(1 - \exp\left(-\frac{\Delta t}{\tau_\mathrm{p}}\right)\right)\tau_\mathrm{p} + \boldsymbol{u}\Delta t + \left(\Delta t - \left(1 - \exp\left(-\frac{\Delta t}{\tau_\mathrm{p}}\right)\right)\tau_\mathrm{p}\right)\boldsymbol{F}_\mathrm{B}\tau_\mathrm{p}, \tag{8}$$

where superscript n and $n+1$ indicate the present and next moment respectively.

Thus, the actual movement of the particle within one time step Δt is obtained: $\Delta x_p = \boldsymbol{x}_\mathrm{p}^{n+1} - \boldsymbol{x}_\mathrm{p}^{n}$. In the CA probabilistic model, it is considered that solid particles are constrained to only move on the same regular lattices as the fluid particles, and a particle at $\boldsymbol{x}_\mathrm{p}$ jumps to a neighboring node at site $\boldsymbol{x}_\mathrm{p} + \boldsymbol{c}_i\Delta t$ with a probability p_i, which is proportional to the projection of the actual displacement of the particle in the direction $\boldsymbol{c}_i$. As a result, the transport probabilities of the particle can be defined as the ratio of projected length of actual displacement to the lattice length along six directions:

$$p_i = \max\left(0, \frac{\Delta\boldsymbol{x}_\mathrm{p}\cdot\mathbf{c}_i}{\Delta x}\right), (i = 1\sim6) \tag{9}$$

where $\mathbf{c}_i$ is the discrete velocity of fluid particles in LBM (see Eq. (2)).

Finally, the particle position after each time step Δt is determined as:

$$\boldsymbol{x}_\mathrm{p}^{n+1} = \boldsymbol{x}_\mathrm{p}^{n} + \mu_1\mathbf{c}_1\Delta t + \mu_2\mathbf{c}_2\Delta t + \mu_3\mathbf{c}_3\Delta t + \mu_4\mathbf{c}_4\Delta t + \mu_5\mathbf{c}_5\Delta t + \mu_6\mathbf{c}_6\Delta t \tag{10}$$

where μ_i is a Boolean variable and equal to 1 with probability p_i.

3. Numerical results and discussion

3.1. Boundary conditions and simulation details

In this three-dimensional simulation, the size of the domain (*i.e.*, the grid resolution in x, y, and z directions) is $128\times64\times64$, which has been proved to be fine enough to obtain reliable flow fields through grid convergence analysis. The gas flow enters into the domain along the x-direction, and the fiber is vertically (z direction) located at the center of the domain. The grid length in all three directions is 1 μm, and the packing density is fixed as 5% in this paper. Therefore the equivalent diameter d_f of elliptical fiber (the diameter of circular fiber with the same volume fraction) is 22.8 μm. Since the length of the simulation domain and the height of the fiber (also the domain) are 128 and 64 μm respectively, the length-to-diameter ratio and the height-to-diameter ratio of the simulation domain with regard to the fiber are 5.6 and 2.8 respectively.

In terms of the boundary conditions, we set the inlet as a constant velocity boundary ($U = 0.1$, 0.2 or 0.3 m/s), the outlet as fully-developed boundary with zero velocity gradient, *i.e.*, , and the other four boundaries as periodic. Non-equilibrium extrapolation scheme is used here to deal with inlet and outlet boundary conditions (Guo, Zheng, & Shi, 2002). The other significant parameters are as following: kinematic viscosity of fluid $\nu = 1.6 \times 10^{-5}$ m^2/s, density of fluid $\rho_0 = 1$ kg/m^3, the ratio of particle density to fluid density $\rho_p/\rho_0 = 1000$. The Re number ($= Ud_f/\nu$) is within the range of 0.1425–0.4275. The air flow (without particles entering the domain) around the elliptical fiber is first simulated by the 3D LB-CA model. When the error of flow fields simulation results, $\sum_{k,j,i} |u^*_{k,j,i} - u_{k,j,i}| / \sum_{k,j,i} |u^*_{k,j,i}|$, is less than 10^{-5}, the flow field is considered as a stable state, where $u_{k,j,i}$ is the fluid velocity of a node indexed by k in z dimension, j in y dimension and i in x dimension, and the asterisk indicates the value of the next time step. Then, the suspended particles are released from the inlet and stream along the x-direction. It is worth nothing that the number concentration of particles at the inlet is kept constant so as to maintain a continuous deposition on the fibers.

In this paper, we only study the operation conditions with a fixed packing density (5%). Different from the simulation of steady-state filtration process, during the non-steady-state filtration process the captured particles can stick on the fiber surface or the particle dendrites and thus influence the flow fields during the particle loading process. Therefore, once one deposited particle is detected, the flow fields will be recalculated. The LB-CA model manages the complex dynamic boundary conditions using very simple rules. Bounce-back boundary condition (bbc) with second-order accuracy is adopted to consider the collision between fluid particles within fluid nodes or boundary nodes and rigid obstacles (fiber or collected particles, which are viewed as solid nodes). In the case of sub-micron particles and low inlet velocity, the bounce effect of captured particles can be ignored (Kasper et al., 2009) and the collision efficiency is equal to the collection efficiency. For more details (including boundary conditions and simulation crafts), readers could refer to our previous publications (Wang et al., 2012, 2014).

Generally speaking, we require 300,000 time steps to obtain sufficient data for analyzing. For each simulation we repeat 3 times to fatigue against the inherent statistic noise of a stochastic simulation. The LB-CA simulations run in a workstation equipped with CPU of Intel(R) Xeon E5-2680 @ 2.7 GHz and memory of 64 GB. The CPU time required is about 16 h for a simulation case.

3.2. The formation process of particle dendrites

For the study of the loading behavior of particles on fibers, the obvious advantage of the simulation method is that not only the complete morphology of the particle dendrites can be obtained, but also the formation process of the particle dendrites can be observed dynamically. However, it is difficult to describe the instantaneous morphology of the particle dendrites by experimental measurements. There are already some conclusions about the morphology of the particle dendrites on circular fibers (Kanaoka, Emi, Hiragi, & Myojo, 1986; Kasper et al., 2009, 2010). When the dominant collection mechanism is inertial impaction, the particles move on straight paths, depositing on the windward of fibers to produce slender structures. If the filtration mechanism is mainly interception, the captured particles will be deposited on the fibers' lateral sides with respect to the stagnation points and increase the fiber's cross-sectional area normal to the flow direction rapidly, leading to a significant increase in collection efficiency and pressure drop. Particle deposition due to Brownian diffusion is believed to form particle dendrites all around the circular fibers, which have higher fractal dimension, being strongly branched and distributed evenly on the fiber surface.

The growth process of particle dendrites on dust loaded elliptical fibers when the particle diameter is 0.4 μm is shown in Fig. 2, which presents clearly three stages of this dynamic process—initial fiber collection, interim fiber-dendrite collection, and complete dendrite collection. At the early stage of filtration process, the particles are relatively uniformly deposited on the surface of the elliptical column fiber, forming some small agglomerates (Fig. 2(a) is for the leeward surface and (b) the windward surface). The first (initial) stage of dendrite formation can be described as a steady-state particle collection process. In the very early stage of the filtration of nearly "clean" fibers, the deposited particles are basically captured by the fibers rather than by particle dendrites. With the increase of captured particles, the small agglomerates grow up to branched dendrites (Fig. 2(c) and (d)). Some deposited particles are captured by the fiber and the others are captured by the particle dendrites in the so-called interim fiber-dendrite collection stage. The growth of particle dendrites changes the distribution of flow field because of the increase of the fiber filtration area, leading to more particles deposit on the windward of the elliptical fiber, especially on the both ends of the elliptical long axis (Fig. 2(c)~(h)). With the further growth of particle dendrites, the deposit particles are basically captured by the dendrite-like clusters in the complete dendrite collection stage.

Fig. 3 displays the formation process of particle dendrites on the surface of a circular fiber for intuitive comparison. Similarly, the non-steady-state filtration process of the circular fiber can be still distinguished three stages: the initial fiber collection, interim fiber-dendrite collection, and complete dendrite collection. Nevertheless, there are some differences when compared with the filtration of the elliptical fiber. Firstly, when looking at the circular and elliptical fibers, there are more particles distributed in the leeward surface of the circular fiber than that of the elliptical fiber; secondly, with respect to the circular fiber, although most of particles are deposited on the windward surface, they are distributed mainly within the range of two stagnation points (Differently, for the elliptical fiber, particles are concentrated on the both ends of the elliptical long axis, especially on the long axis end more approaching to the flow inlet). Thirdly, within the same time period the circular fiber captures fewer particles than the elliptical fiber.

Fig. 4 shows the 2-dimentional particle dendrites structures loaded on the elliptical fibers and the circular fibers at some specified sections of z direction. Basically, with respect to one specified section, the particle dendrites are distributed more homogeneously on the circular fiber surface than on the elliptical fiber. On the other side, it is clearly shown that the particle dendrites are not distributed homogeneously in the z (vertical) direction (*i.e.*, the fiber axial direction which is normal to the computational domain of the 2D simulation). The growth of particle dendrites in all 3 dimensions depends on complex flow-particle-fiber interaction. Although

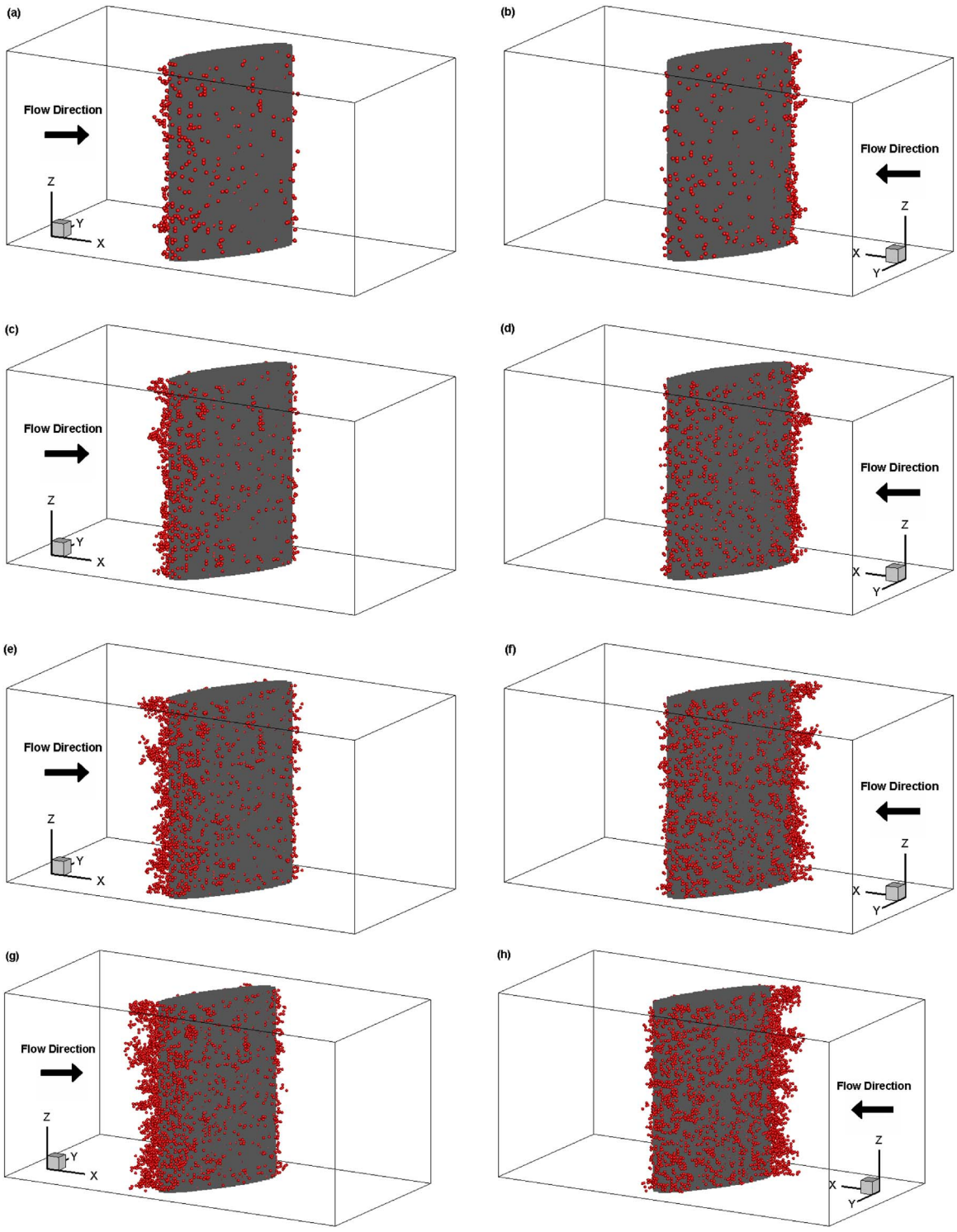

Fig. 2. The formation process of particle dendrites on the surface of an elliptical fiber (the equivalent diameter d_f of elliptical fiber is 22.8 μm, particle diameter $d_p = 0.4$ μm, inlet flow velocity is 0.1 m/s, aspect ratio of the elliptical fiber is 4, orientation angle is 60°). (a) and (b): at the 20000th time step, when the number of captured particles is 633; (c) and (d): at the 40000th time step with 1668 particles captured; (e) and (f): the 60000th time step with 2837 particles captured; (g) and (h): the 80000th time step with 3944 particles captured. (a), (c), (e) and (g) are for the leeward surface; (b), (d), (f) and (h) are for the windward surface.

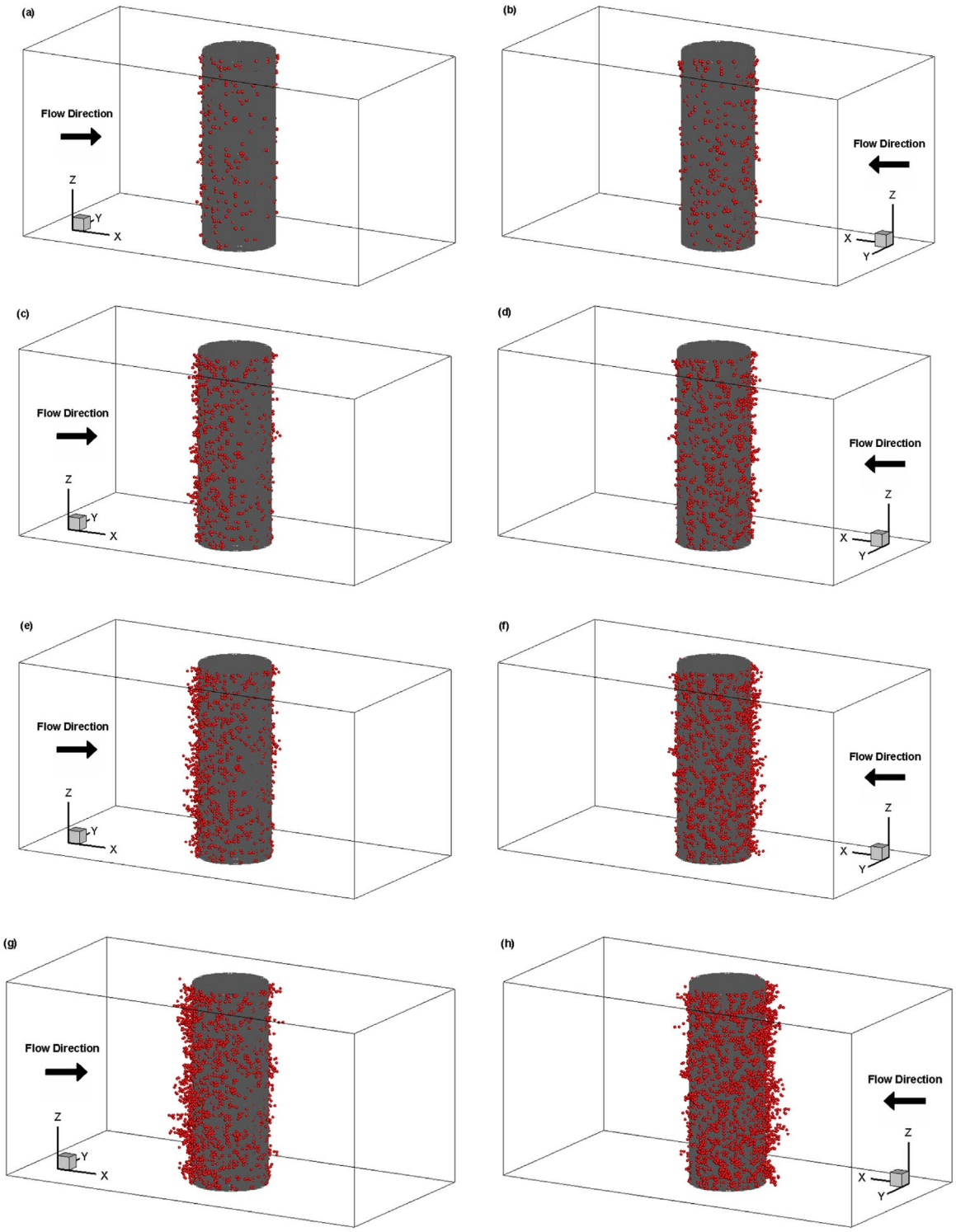

Fig. 3. The formation process of particle dendrites on a circular fiber surface (the diameter of the circular fiber is 22.8 μm, particle diameter $d_p = 0.4$ μm, inlet flow velocity is 0.1 m/s). (a) and (b): at the 20000th time step, when the number of captured particles is 547; (c) and (d): at the 40000th time step with 1416 particles captured; (e) and (f): the 60000th time step with 2299 particles captured; (g) and (h): the 80000th time step with 3309 particles captured. (a), (c), (e) and (g) are for the leeward surface; (b), (d), (f) and (h) are for the windward surface.

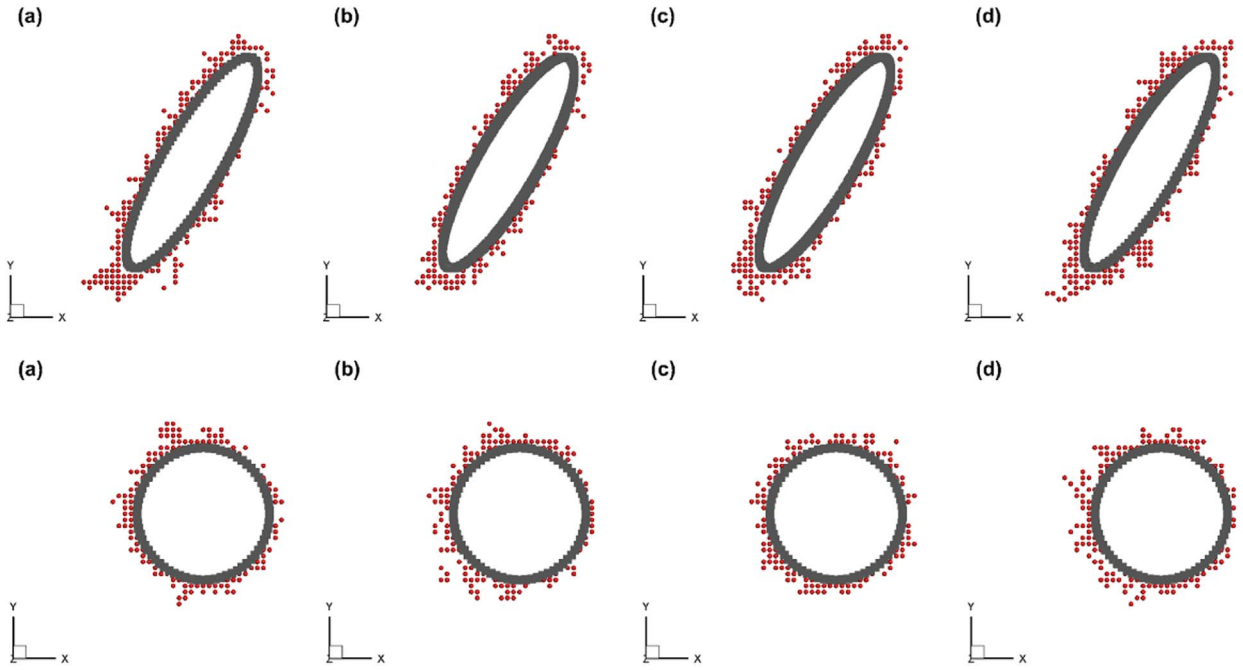

Fig. 4. The 2-dimentional particle dendrites structures loaded on the elliptical fibers and the circular fibers at some specified sections of z direction. (a) $z=8$; (b) $z=24$; (c) $z=40$; (d) $z=56$. Calculation condition: the (equivalent) diameter of the fibers is 22.8 μm, particle diameter $d_p=0.4$ μm, inlet flow velocity is 0.1 m/s, aspect ratio and orientation angle of the elliptical fiber are 4 and 60° respectively; at the 60000th time step, the number of captured particles is 2837 for the elliptical fiber and 2299 for the circular fiber.

the 2D image from the 2D simulation is generally viewed as a typical representation of real 3D image, the particle dendrites are also branched in the z direction, which results in quite different dendrites structure at different sections. Therefore, the 2D results are qualitative at best, and it is essential to simulate the non-steady-state filtration processes of fibers using 3-dimensitonal numerical models and methods. It is worth noting that the dendrites may stretch vertically to neighboring sections, resulting in some scattered particle or particle clusters on a specified section.

In order to make a quantitative comparison to the capture efficiencies of the elliptical fiber and circular fibers, we calculate the absolute capture efficiency of a fiber when capturing the same number of particles. As shown in Table 1, the absolute capture efficiency of the elliptical fiber is often higher than that of the circular fiber. At the same time, with the increase of the aspect ratio of elliptical fibers, the capture efficiency increases as well.

As mentioned above, the formation and growth of particle dendrites will influence the flow fields, which will then influence the particle motion and also the particle filtration by the fibers or particle dendrites. It is the so-called fluid-particle-fiber interaction. Fig. 5 shows the flow fields around the elliptical fibers (as well the particle deposits) at the specified section of $z=32$. As the dendrites grow larger, the local flow velocity near the deposits increases. As a result, the *Pe* number of particles approaching the fiber increases, which weakens the diffusion ability of particles. That is to say, these particles are much more difficult to move to the leeward of the fiber and more particles are deposited on the windward of the fiber. On the other side, the interception mechanism also influences the particle deposition, which results in more and more particles are deposited on both ends of the elliptical long axis (also the stagnation points for the elliptical fibers).

Fig. 6 shows the complete morphologies of the particle dendrites with different particle sizes (0.3–0.5 μm) on the surface of elliptical fibers. It can be seen that these particle dendrites in Fig. 6 have very similar structure. Furthermore, Fig. 7 shows the number distribution of deposited particles on the fiber surface with different particle size, where N_θ is the number of deposited particles within a specified angular range (here the X-axis is set on the elliptical long axis and the Y-axis is set on the elliptical short axis), N is

Table 1
The capture efficiency of elliptical fibers with different aspect ratios. ε of 1 means the circular fiber. η_{2000} is the capture efficiency when capturing 2000 particles; et cetera. $d_f=22.8$ μm, $d_p=0.4$ μm, inlet flow velocity is 0.1 m/s, orientation angle (for elliptical fibers) is 60°.

Aspect ratio (ε)	η_{2000}	η_{4000}	η_{6000}
1	0.101	0.114	0.127
2	0.105	0.122	0.136
3	0.111	0.126	0.138
4	0.116	0.135	0.147

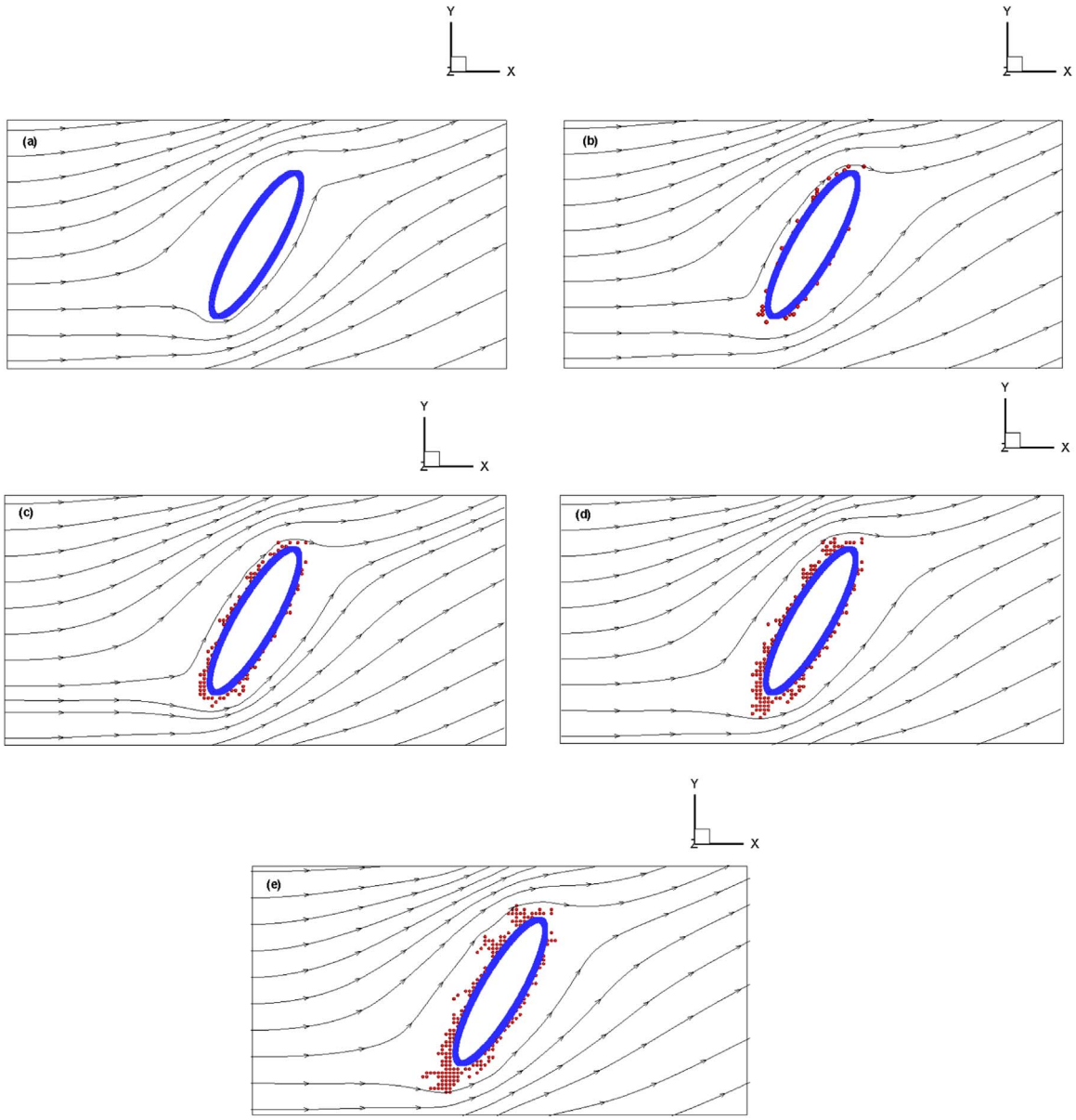

Fig. 5. The particle dendrites structures and flow fields at a specified section ($z = 32$) of z direction ($d_f = 22.8$ μm, $d_p = 0.4$ μm, inlet flow velocity is 0.1 m/s, aspect ratio is 4, orientation angle is 60°). (a) the flow field around a clean elliptical fiber; (b) at the 20000th time step, when the number of captured particles is 633; (c) the 40000th time step with 1668 particles captured; (d) the 60000th time step with 2837 particles captured; (e) the 80000th time step with 3944 particles captured.

the total number of deposited particles. It can be seen from the figure that the distribution of particles with different particle diameters is substantially consistent. Kanaoka et al. (1986) and Guo et al. (2002) also concluded that the morphologies of particle dendrites formed on the surface of the fibers are similar when the dominant filtration mechanism is the same. Generally, the structure of particle dendrites presents as a combined feature of the dendrites due to pure Brownian diffusion and those caused by pure interception. Nevertheless, as particle size increases, more particles deposit on the end of elliptical long axis approaching to the flow inlet. It is because the interception effect is enhanced for larger particles (*i.e.*, 0.5 μm).

3.3. The dynamic evolution of both pressure drop and collection efficiency of elliptical fibers during loading

As mentioned in Section 3.2, during the particles loading process, the dendrite structures on the fiber change the filtration area, leading to an increase of pressure drop and collection efficiency. Reasonable design and optimization of fibrous filters need good understanding on the particle loading process. In this section, we investigate the dynamic evolution of both pressure drop and collection efficiency of elliptical fibers during clogging.

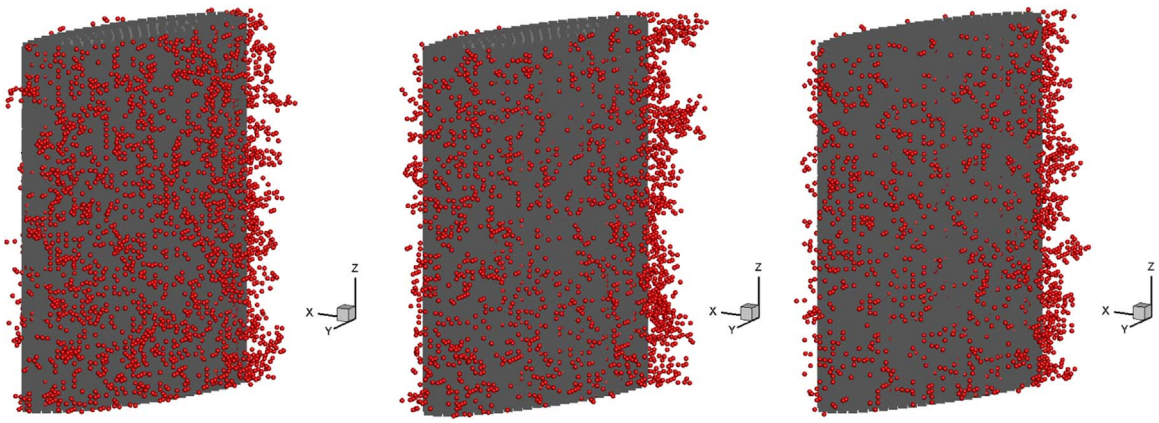

Fig. 6. The complete morphologies of the particle dendrites with different particle size (from left to right, d_p is 0.3, 0.4 and 0.5 μm respectively; inlet flow velocity is 0.1 m/s, the equivalent diameter of elliptical fiber is 22.8 μm, aspect ratio is 4, orientation angle is 60°; at the 60000th time step when capturing 3698 particles of 0.3 μm, 2837 particles of 0.4 μm, and 2082 particles of 0.5 μm).

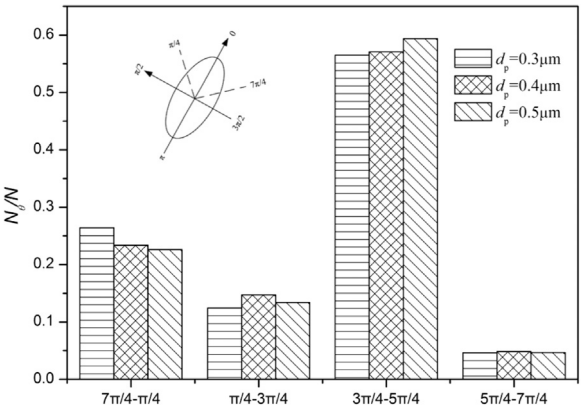

Fig. 7. Number distribution of deposited particles on the fiber surface with different particle size (inlet flow velocity is 0.1 m/s, the equivalent diameter of elliptical fiber is 22.8 μm, aspect ratio is 4, orientation angle is 60°; at the 60000th time step when capturing 3698 particles of 0.3 μm, 2837 particles of 0.4 μm, and 2082 particles of 0.5 μm).

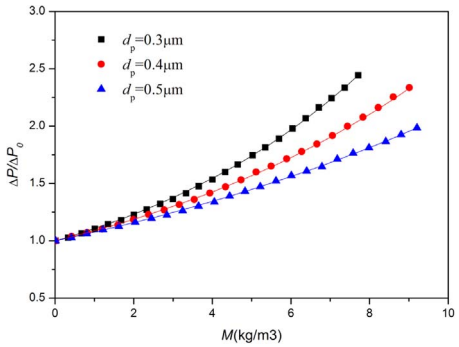

Fig. 8. Dynamic changes of the normalized pressure drop for different particle diameters (inlet flow velocity is 0.1 m/s, d_f = 22.8 μm, aspect ratio is 4, orientation angle is 60°).

Fig. 8 demonstrates the pressure drop of dust loaded elliptical fibers ΔP normalized by the corresponding pressure drop of clean elliptical fibers ΔP_0 with different particle diameters during particle loading. The X-axis in the plots is the mass of captured particles in kilograms divided by the fiber volume. The increase in the pressure drop is ascribed to the increase in the filtration area and the change in the shape of the filtration media. As shown in Fig. 8, the increase rate of the normalized pressure drop is higher for smaller particles when plotted against the mass of captured particles. Similar conclusions have been obtained in other studies for the non-steady-state filtration on circular fibers (Hosseini & Tafreshi, 2012; Thomas et al., 1999, 2001).

Fig. 9 presents the logarithmic scaling of the normalized pressure drop *vs.* the mass of deposited particles. $\ln(P/P_0)$ presents a

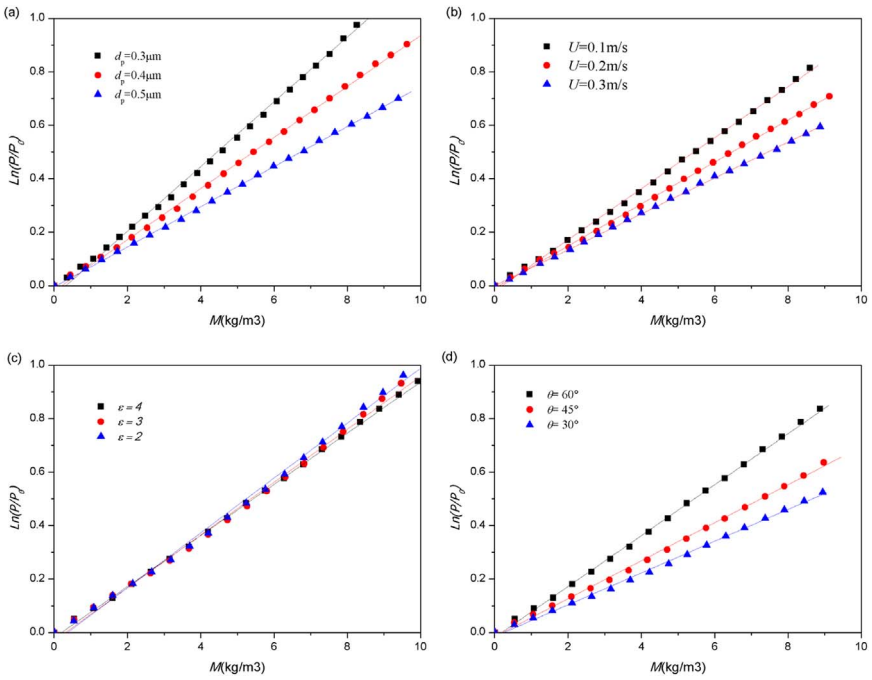

Fig. 9. The logarithmic scaling of the normalized pressure drop as a function of the deposit mass under various filtration conditions. (a) for different particle diameters; (b) for different inlet flow velocities; (c) for different aspect ratios; (d) for different orientation angles. If not specified, d_f is 22.8 μm, d_p is 0.4 μm, inlet flow velocity is 0.1 m/s, aspect ratio of elliptical fibers is 4, orientation angle is 60° in these simulations.

linear relationship with the deposit mass. Therefore, it is possible to fit these data by

$$\Delta P/\Delta P_0 = \varphi \cdot e^{M/h} + \xi. \tag{11}$$

When there is no particle depositing on the fiber, the normalized pressure drop of elliptical fiber is 1. Therefore, when $M = 0$, $\Delta P/\Delta P_0 = 1$, so $\xi + \varphi = 1$. The equation can be transferred to:

$$\frac{(\Delta P - \Delta P_0)}{\Delta P} = \varphi \cdot (e^{M/h} - 1) \tag{12}$$

Fig. 9 also presents that the normalized pressure drop also increases exponentially with the deposit mass for different inlet flow velocities, different orientation angles, and different aspect ratios. The increase rate of the normalized pressure drop is higher for a smaller inlet flow velocity, or a smaller aspect ratio, or a larger orientation angle, when plotted against the mass of captured particles.

Fig. 10 demonstrates the collection efficiency of dust loaded elliptical fibers (η) normalized by the collection efficiency of the clean fibers (η_0) under various filtration conditions during particle loading. If not specified, d_f is 22.8 μm, d_p is 0.4 μm, inlet flow velocity is 0.1 m/s, aspect ratio of elliptical fibers is 4, orientation angle is 60° in these simulations. The simulation results show that the normalized efficiency increases with the mass of the captured particles. However, the increase rate of normalized collection efficiency does not remain constant, which is different from the expression given by Kanaoka et al. (1980). The increase rate of normalized efficiency decreases with increasing M and then reaches a constant value, resulting in a linear relationship as shown in Fig. 10, which is consistent with the conclusion of Hosseini and Tafreshi (2012). Kasper et al. (2009) also found similar results in their experiments with large particles. It can be explained that the growth of filtration area relative to its original area is faster at the initial stages of the particle loading process. The particle size, inlet flow velocity, aspect ratio and orientation angle of elliptical fiber affect the onset of the linear region. In this work, the curve fitting just contains the linear portion of the plots shown in Fig. 10. The normalized collection efficiency of elliptical fibers can be modelled as

$$\eta/\eta_0 = \gamma + \lambda M. \tag{13}$$

A larger value of λ means a faster increase of the normalized collection efficiency. Generally, λ decreases as the particle size, the inlet flow velocity and the aspect ratio increases, while increases as the orientation angle. Obviously, it is similar to the evolution of the normalized pressure drop: a smaller particle size, inlet velocity, or aspect ratio leads to a larger increase rate of the normalized pressure drop, while a larger orientation angle results in a faster increase of the normalized pressure drop. There may exist inherent relation between the two parameters (h and λ), which deserves further investigation.

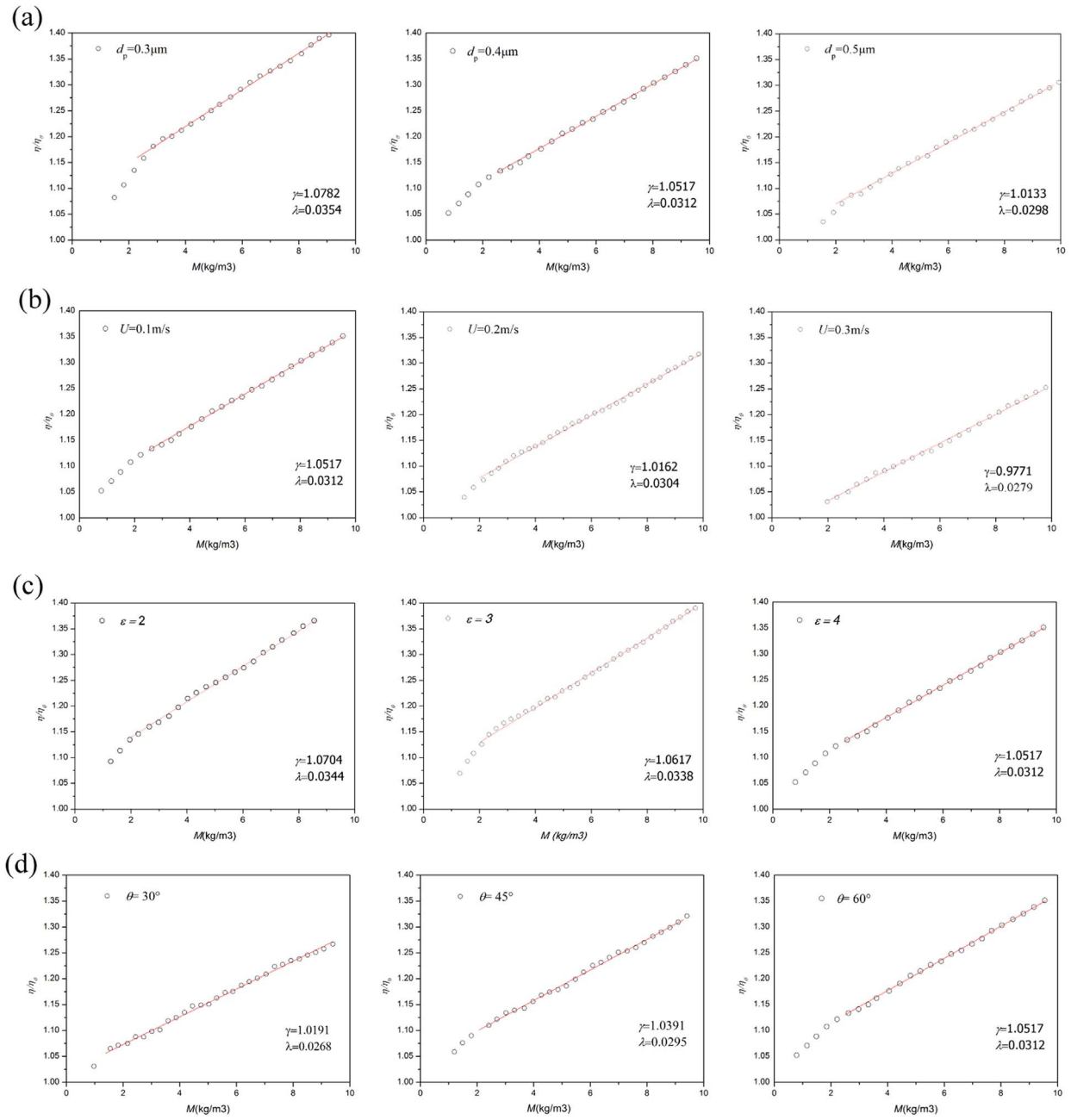

Fig. 10. Dynamic changes of the normalized collection efficiency under various filtration conditions. (a) different particle diameters; (b) different inlet flow velocities; (c) different aspect ratios of elliptical fibers; (d) different orientation angles of elliptical fibers.

4. Conclusions

The particle loading behavior and the dynamic evolution of filtration performance of elliptical fibers are investigated using the lattice Boltzmann-cellular automata (LB-CA) probabilistic model, including the growth process and morphological analysis of the particle dendrites. The dynamic evolution processes of both pressure drop and collection efficiency with the increase of deposit mass are quantitatively analyzed. These results are useful for the design and optimization of the fibrous filter structure.

The captured particles of 0.3–0.5 μm in diameter (in the “Greenfield gap” range) deposit on the surface of the elliptical fiber relatively uniformly at the initial stage of loading process. The deposited particle leads to the formation of complicated dendrites, expanding the filtration area and thereby altering the flow field. Particles will mostly deposit on the windward of the elliptical fibers at the complete dendrites capture stage, especially on the both ends of the elliptical long axis. The particle dendrites grow in all 3 directions and also disturb the flow fields in all 3 directions. It is necessary to three-dimensionally characterize the particle dendrites

structure and the non-steady-state filtration processes either numerically or experimentally. From the three-dimensional LB-CA simulation, it is found that the normalized pressure drop and the normalized capture efficiency increase exponentially and linearly as the deposit mass, respectively.

Acknowledgements

This study was financially supported by the National Natural Science Foundation of China (51522603, 51390494). We also thanks Dr. Jianlong Wan (HUST) for his help in drawing these 3D images.

References

Adamiak, K. (1999). Viscous flow model for charged particle trajectories around a single square fiber in an electric field. *IEEE Transactions on Industry Applications, 35*, 352–358.
Billings, C. E. (1996). *Effects of particle accumulation in aerosol filtration.* Ph.D. ThesisCalifornia Institute of Technology.
Brown, R. C. (1993). *Air filtration: An integrated approach to the theory and applications of fibrous filters.* Oxford, England: Pergamon Press.
Cheung, C., Cao, Y., & Yan, Z. (2005). Numerical Model for particle deposition and loading in electret filter with rectangular split-type fibers. *Computational Mechanics, 35*(*6*), 449–458.
Fardi, B., & Liu, B. Y. H. (1992). Flow field and pressure drop of filters with rectangular fibers. *Aerosol Science and Technology, 17*, 36–44.
Filippova, O., & Hänel, D. (1997). Lattice-Boltzmann simulation of gas-particle flow in filters. *Computers & Fluids, 26*, 697–712.
Fotovati, S., Tafreshi, H. V., & Pourdeyhimi, B. (2011). Analytical expressions for predicting performance of aerosol filtration media made up of trilobal fibers. *Journal of Hazardous Materials, 186*(*2*), 1503–1512.
Greenfield, S. (1957). Rain scavenging of radioactive particulate matter from the atmosphere. *Journal of Meteorology, 14*, 115–125.
Guo, Z., Zheng, C., & Shi, B. (2002). Non-equilibrium extrapolation method for velocity and pressure boundary conditions in the lattice Boltzmann method. *Chinese Physics, 11*, 366–374.
Hosseini, S., & Tafreshi, H. V. (2011). On the importance of fibers' cross-sectional shape for air filters operating in the slip flow regime. *Powder Technology, 212*(*3*), 425–431.
Hosseini, S. A., & Tafreshi, H. V. (2012). Modeling particle-loaded single fiber efficiency and fiber drag using ANSYS-fluent CFD code. *Computers & Fluids, 66*, 157–166.
Huang, H. K., Wang, K., & Zhao, H. B. (2016). Numerical study of pressure drop and diffusional collection efficiency of several typical noncircular fibers in filtration. *Powder Technology, 292*, 232–241.
Inagaki, M., Sakai, K., Namiki, N., et al. (2001). Influence of fiber cross-sectional shape on filter collection performance. *Kagaku Kogaku Ronbunshu, 27*(*1*), 113–120.
Kanaoka, C., Emi, H., Hiragi, S., & Myojo, T. (1986). *Morphology of particulate agglomerates on a cylindrical fiber and collection efficiency of a dust loaded fiber.* In Aerosols formation and reactivity (Proceedings 2nd international aerosol conferenceOxford: Pergamon Journals Ltd674–677.
Kanaoka, C., Emi, H., & Myojo, T. (1980). Simulation of the growing process of a particle dendrite and evaluation of a single fiber collection efficiency with dust load. *Journal of Aerosol Science, 11*, 377–389.
Kanaoka, C., & Hiragi, S. (1990). Pressure drop of air filter with dust load. *Journal of Aerosol Science, 21*, 127–137.
Kasper, G., Schollmeier, S., & Meyer, J. (2010). Structure and density of deposits formed on filter fibers by inertial particle deposition and bounce. *Journal of Aerosol Science, 41*, 1167–1182.
Kasper, G., Schollmeier, S., Meyer, J., & Hoferer, J. (2009). The collection efficiency of a particle-loaded single filter fiber. *Journal of Aerosol Science, 40*, 993–1009.
Lamb, G. E. R., & Costanza, P. A. (1980). Influences of fiber geometry on the performance of nonwoven air filters: Part III: Cross-sectional shape. *Textile Research Journal, 50*(*6*), 362–370.
Lantermann, U., & Hänel, D. (2007). Particle Monte Carlo and lattice-Boltzmann methods for simulations of gas–particle flows. *Computers & Fluids, 36*, 407–422.
Li, S. Q., & Marshall, J. S. (2007). Discrete element simulation of micro-particle deposition on a cylindrical fiber in an array. *Journal of Aerosol Science, 38*(*10*), 1031–1046.
Masselot, A., & Chopard, B. (1998). A lattice Boltzmann model for particle transport and deposition. *Europhysics Letters, 42*, 259–264.
Maze, B., Vahedi Tafreshi, H., Wang, Q., & Pourdeyhimi, B. (2007). A simulation of unsteady-state filtration via nanofiber media at reduced operating pressures. *Journal of Aerosol Science, 38*, 550–571.
Myojo, T., Kanaoka, C., & Emi, H. (1984). Experimental observation of collection efficiency of a dust-loaded fiber. *Journal of Aerosol Science, 15*, 483–489.
Ouyang, M., & Liu, B. Y. H. (1998). Analytical solution of flow field and pressure drop for filters with rectangular fibers. *Journal of Aerosol Science, 29*, 187–196.
Payatakes, A. C., & Gradoń, L. (1980). Dendritic deposition of aerosol particles in fibrous media by inertial impaction and interception. *Chemical Engineering Science, 35*, 1083–1096.
Payatakes, A. C., & Tien, C. (1976). Particle deposition in fibrous media with dendrite-like pattern: A preliminary model. *Journal of Aerosol Science, 7*(*2*), 85–100.
Przekop, R., & Gradoń, L. (2008). Deposition and filtration of nanoparticles in the composites of nano-and microsized fibers. *Aerosol Science and Technology, 42*, 483–493.
Przekop, R., Moskal, A., & Gradoń, L. (2003). Lattice-Boltzmann approach for description of the structure of deposited particulate matter in fibrous filters. *Journal of Aerosol Science, 34*, 133–147.
Qian, Y. H., D'Humieres, D., & Lallemand, P. (1992). Lattice BGK models for Navier-Stokes equation. *Europhysics Letters, 17*, 479–484.
Ramarao, B. V., Tien, C., & Mohan, S. (1994). Calculation of single fiber efficiencies for interception and impaction with superposed brownian motion. *Journal of Aerosol Science, 25*(*2*), 295–313.
Raynor, P. C. (2002). Flow field and drag for elliptical filter fibers. *Aerosol Science and Technology, 36*, 1118–1127.
Sanchez, J. R., Rodriguez, J. M., Alvaro, A., et al. (2007). The capture of fly ash particles using circular and noncircular cross-section fabric filters. *Environmental Progress, 26*(*1*), 50–58.
Thomas, D., Contal, P., Renaudin, V., Penicot, P., Leclerc, D., & Vendel, J. (1999). Modelling pressure drop in hepa filters during dynamic filtration. *Journal of Aerosol Science, 30*, 235–246.
Thomas, D., Penicot, P., Contal, P., Leclerc, D., & Vendel, J. (2001). Clogging of fibrous filters by solid aerosol particles Experimental and modelling study. *Chemical Engineering Science, 56*, 3549–3561.
Wang, H., Zhao, H., Guo, Z., & Zheng, C. (2012). Numerical simulation of particle capture process of fibrous filters using Lattice Boltzmann two-phase flow model. *Powder Technology, 227*, 111–122.
Wang, H., Zhao, H., Wang, K., He, Y., & Zheng, C. (2013). Simulation of filtration process for multi-fiber filter using the Lattice-Boltzmann two-phase flow model. *Journal of Aerosol Science, 66*, 164–178.
Wang, H. M., Zhao, H. B., Wang, K., et al. (2014). Simulating and modeling particulate removal processes by elliptical fibers. *Aerosol Science and Technology, 48*, 207–218.
Wang, K., & Zhao, H. B. (2015). The influence of fiber geometry and orientation angle on filtration performance. *Aerosol Science and Technology, 49*(*2*), 75–85.
Zhao, Z. M., Tardos, G. I., & Pfeffer, R. (1991). Separation of airborne dust in electrostatically enhanced fibrous filters. *Chemical Engineering Communications, 108*, 307–332.
Zhu, C., Lin, C. H., & Cheung, C. S. (2000). Inertial impaction-dominated fibrous filtration with rectangular or cylindrical fibers. *Powder Technology, 112*(*1*), 149–162.